Chirped Delay Lines in Microstrip Technology

M. A. G. Laso, *Student Member, IEEE*, T. Lopetegi, *Student Member, IEEE*, M. J. Erro, *Student Member, IEEE*, D. Benito, M. J. Garde, M. A. Muriel, *Senior Member, IEEE*, M. Sorolla, *Senior Member, IEEE*, and M. Guglielmi, *Senior Member, IEEE*

***Abstract*—In this paper, we report on a design method for chirped delay lines (CDLs) in microstrip technology. They consist in a continuously varying strip width, so that the coupling location between the quasi-TEM microstrip mode and the same but counter-propagating mode is linearly distributed in frequency. High delay × bandwidth products, over frequency ranges of several gigahertzs, can be obtained following this procedure. Experimental data confirm the design method. Real-time Fourier analysis of wideband pulses can be performed using these CDLs.**

***Index Terms*—Chirped Bragg coupling, chirped delay line, impedance modulation, microstrip technology, quadratic-phase filter.**

I. Introduction

A CHIRPED delay line (CDL) is a quadratic-phase filter whose frequency response $H(\omega) = A_0(\omega) \cdot \exp(-j \cdot \varphi_0(\omega))$, around a central frequency ω_0, is characterized by uniform insertion losses, $A_0(\omega)$, and a linear group-delay, $\varphi_0 = d\varphi_0/d\omega$, across the operating frequency-band. Different approaches have been followed to produce CDLs, mainly as components of compressive receivers [1]. Some of them are not simple to fabricate, while other ones do not meet easily the design specifications. In this paper, we report on a plain design method for CDLs in microstrip lines with continuously varying strip width to achieve closely the required frequency features, that is, the desired frequency range, delay versus frequency slope, and input/output impedance, and benefiting from fabrication on a mature technology and compatibility with monolithic circuits. This way, CDLs with very high time-bandwidth products (defined as the total delay excursion times the bandwidth), over ranges of several gigahertz, can be obtained on high-dielectric-constant- and thin substrates. Promising applications as the real-time spectral analysis of wideband signals can be envisaged using these devices.

II. Microstrip CDL Design

Let the characteristic impedance of a microstrip line be changed by a continuously changing profile, for example a nonuniform microstrip line with continuously varying strip width following a linearly frequency-modulated (chirped) continuous periodic function. Then, the phase-matching condition for resonant Bragg coupling between the quasi-TEM microstrip mode and the same but counter-propagating mode is ideally satisfied at only one position for each spectral frequency, from which it will be back-reflected. In fact, if the perturbation is linearly chirped then we will see that the mode-coupling location varies linearly in frequency and, as result, the reflection time is also a linear function of frequency.

Consider $Z_0(z)$ as the perturbed microstrip impedance given by $Z_0(z) = f_{\zeta(z)}(z)$, where $\zeta(z)$ represents the modulation of the local spatial angular frequency of a continuous periodic function $f(z)$, and z is the axis along which the microstrip CDL is extended from $z = -L/2$ to $z = L/2$, being L the device total length. We will show next that if $\zeta(z) = \zeta_0 + 2 \cdot C \cdot z$, then $Z_0(z)$ yields a mode-coupling location linearly distributed in spectral frequency. The parameter $C(m^{-2})$ fixes the variation rate of the local spatial frequency and $\zeta_0 = \zeta(z = 0)$ is the value of the local spatial frequency at the device central point.

The Bragg condition states that the perturbation period for an angular frequency ω to be coupled to the counter-propagating quasi-TEM mode in a microstrip line can be estimated as $\lambda_g/2$ (π-rad phase-shift), being λ_g the guided wavelength at this frequency in the unperturbed (constant strip width) microstrip line [2]. Then, in the quasistatic (TEM) approximation, the angular frequency locally reflected at $z, \omega_l(z)$, is found as

$$\omega_l(z) = \frac{\zeta(z) \cdot c}{2 \cdot \sqrt{\varepsilon_{\text{eff}}|_{50\Omega}}} = \frac{c}{2 \cdot \sqrt{\varepsilon_{\text{eff}}|_{50\Omega}}} \cdot \left(\frac{2\pi}{a_0} + 2Cz\right) \propto z \tag{1}$$

if an impedance modulation around 50 Ω is considered. $\varepsilon_{\text{eff}}|_{50\,\Omega}$ is the effective dielectric constant for a 50 Ω-line at low-frequency regime, c is the speed of light in vacuum, and $a_0 = 2\pi/\zeta_0$ is the local spatial period at $z = 0$, which fixes the central operation frequency ω_0. Equation (1) anticipates that a linear spatial frequency modulation of the impedance provides a linear group delay in a bandwidth $\Delta\omega = |\omega_l(z = L/2) - \omega_l(z = -L/2)| = c \cdot |C| \cdot L/\sqrt{\varepsilon_{\text{eff}}|_{50\,\Omega}}$, around a central frequency $\omega_0 = c \cdot \pi/(a_0 \cdot \sqrt{\varepsilon_{\text{eff}}|_{50\,\Omega}})$, and with a delay slope $|\ddot{\varphi}_0| = 2\sqrt{\varepsilon_{\text{eff}}|_{50\,\Omega}} \cdot L/(c \cdot \Delta\omega)$, in units of s^2/rad, whose sign is the same as the sign of C. The delay slope is derived by taking into account that $\Delta\omega \cdot |\ddot{\varphi}_0|$ is the time-delay difference between the arrivals at the input of the extreme frequencies of the bandwidth, $\omega_l(z = -L/2)$ and $\omega_l(z = L/2)$, the former reflected at the input and the latter at the output of the device, respectively (path difference = 2·CDL length). Once the device length, L, and the variation rate of

Manuscript received July 10, 2001; revised September 19, 2001. This work was supported by the Gobierno de Navarra and the Spanish CICYT under Projects TIC2001-2969-C03-03, TIC2001–3061, and TIC 99-0292. The review of this letter was arranged by Associate Editor Dr. Arvind Sharma.

M. A. G. Laso, T. Lopetegi, M. J. Erro, D. Benito, M. J. Garde, and M. Sorolla are with the Electronic Engineering Department, Public University of Navarre, Campus Arrosadía, Pamplona, Spain.

M. A. Muriel is with the Polytechnic University of Madrid, Ciudad Universitaria, Madrid, Spain.

M. Guglielmi is with the RF Systems Division, AG Noordwijk, The Netherlands.

Publisher Item Identifier S 1531-1309(01)11123-2.

the local spatial frequency, C, in $f_{\zeta(z)}(z)$ have been fixed, we can straightforwardly test these design relationships by obtaining the loss-less behavior of the CDL, which provides valid information on the approximated operation frequency range and delay characteristic, by means of

$$dS_{11}/dz - 2\cdot\gamma\cdot S_{11} + \frac{1}{2}\cdot\left(1 - S_{11}^2\right)\cdot d(\ln(Z_0))/dz = 0 \quad (2)$$

derived from the differential equations for voltage, V, and current, I, in a transmission line model [3], and solving S_{11} for the input port, $z = -L/2$, being $S_{11} = (V/I - Z_0)/(V/I + Z_0)$ the reflection coefficient and taking a purely imaginary propagation constant $\gamma = j\cdot\beta = j\cdot\omega\cdot\sqrt{\varepsilon_{\text{eff}}}/c$ (ε_{eff} depends only on the strip width, for a given substrate, in the quasistatic approximation). Eq. (2) can readily be integrated numerically, taking into account that at the endpoint the reflection coefficient is supposed to be zero due to perfect matching.

The function $f(z)$ is chosen to minimize the frequency interference of the spurious reflected bands, at the harmonics of ω_0, on the main band since low-rippled response is a requirement for a CDL. If $f(z) = 50\cdot\exp(\sin(2\pi\cdot z/a_0))$ for a nonchirped impedance modulation (i.e., $Z_0(z) = f(z)$) around 50 Ω with a spatial periodicity a_0, then $S_{11}(\omega, z = -L/2)$ can be analytically shown, using (2), to be a single-frequency-tuned response mainly confined in the nearness of the central frequency ω_0, provided that $L \gg a_0$ for high time-bandwidth products. Any other election of the periodic function $f(z)$ would have led to frequency responses with reflected bands at $2\cdot\omega_0, 3\cdot\omega_0, \ldots$, although, if $f(z)$ is continuous and smooth, these replicas would be likely constrained to reduced levels [4]. Therefore, the impedance modulation finally implemented is

$$\begin{aligned} Z_0(z) &= 50\cdot\exp\left(A\cdot W(z)\cdot\sin\left(\int\zeta(z)\cdot dz\right)\right) \\ &= 50\cdot\exp(A\cdot W(z)\cdot\sin(2\pi/a_0\cdot z \\ &\quad + C\cdot z^2 - C\cdot L^2/4)) \end{aligned} \quad (3)$$

where A (nondimensional) is an amplitude factor and the integration constant is fixed to $-C\cdot L^2/4$ for 50 Ω-input and output ports when L is a multiple of $a_0\cdot W(z)$ is a windowing function for smoother input and output impedance transitions to avoid partially reflections from the extremes of the structure that give rise to different long-path Fabry–Perot like resonances, which cause undesirable rapid ripple to appear around the mean values in the magnitude and group-delay versus frequency patterns degrading the CDL performance. Furthermore, both negative values of C, which imply upper (higher loss) frequencies to be reflected in first place, and asymmetric $W(z)$, which compensates for the longer lossy round trips of lower frequencies (conductor losses, $\propto\sqrt{\omega}$, are much more significant than dielectric losses, $\propto\omega$, for most microstrip substrates), can be proved to lead to better equalized reflection losses across the operation band if full-wave electromagnetic simulations are performed (in our case using the commercially available *Agilent (tm) Momentum* software). Parasitic effects in microstrip-like radiation losses and surface-wave propagation are maintained within negligible values due to the smooth rounded strip shape.

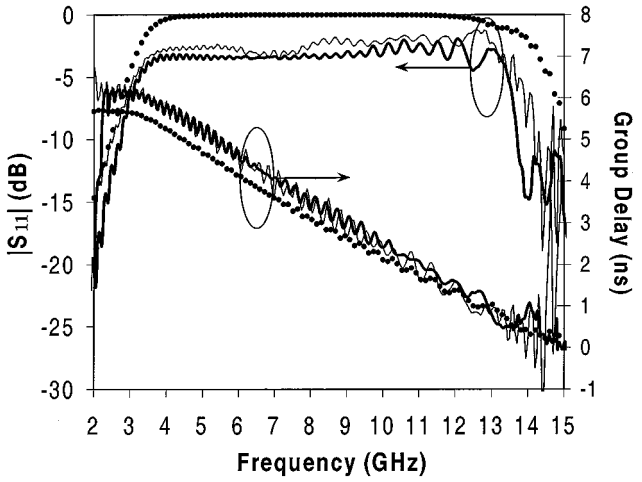

Fig. 1. S_{11}-parameter of the microstrip CDL (magnitude, left axis; and group delay, right axis) obtained by loss-less quasistatic approximation (dotted line), commercial software (thin solid line), and measurement (thick solid line).

III. Numerical and Experimental Results Discussion

In this section, we present an example of microstrip CDL with linearly chirped impedance modulation around 50 Ω using a medium quality *Rogers (tm) RO3010* substrate ($\varepsilon_r = 10.2$, and thickness $h = 1.27$ mm). The design frequency characteristics are: operation around 9 GHz, 12 GHz-bandwidth, and -0.5 ns/GHz ($\ddot{\varphi}_0 \cong -0.08$ ns^2/ rad)-delay slope. The next parameter set fulfills the response: $a_0 = 6.4$ mm, $L = 50\cdot a_0$, and $C = -2080$ m^{-2}. The asymmetric tapering function $W(z)$ is gaussian $W(z) = \exp(-4\cdot((z - L/4)/L)^2)$, and $A = 0.4$.

Once all the parameters in (3) have been fixed, we implement the impedance variation as a strip width modulation (see [5], for instance). As the impedance varies between 35 and 75 Ω, the strip width changes between 0.5 and 2.5 mm approximately. In Fig. 1, the S_{11} parameter obtained by (2) in a lossless and quasistatic approximation (dotted line) is compared with the simulation employing the commercial software (thin solid line) and the measurement of the prototype (thick solid line), showing that the CDL provides the required features of flat magnitude and linear group delay. The reflection losses are maintained around -3 dB over the entire bandwidth (dielectric loss tangent, $\tan\delta = 0.0026$, and metal conductivity $\sigma = 5.8\cdot 10^7$ S/m). We decided to use an appropriate time-gating to subtract the mismatch effects of the connectors in the presented measurement because these effects are critical in broadband operation and, in the intended integrated solution, the input and output sections will be also microstrip lines.

Fig. 2 shows the average internal power distribution, as relative brightness levels, for every frequency in the operation bandwidth as a function of the position in the CDL, $|A^+(z)|^2 + |A^-(z)|^2$, being $A^\pm$ the complex amplitudes of the quasi-TEM mode traveling in the forward $(+)$ and backward $(-)$ z-direction. These values verify that $A^-/A^+ = S_{11}$, and they are related to the voltage and current along the transmission-line model [3], [6]. A coupling-location linearly distributed in frequency is clearly observed as well as higher frequencies being reflected back earlier than lower ones (negative C).

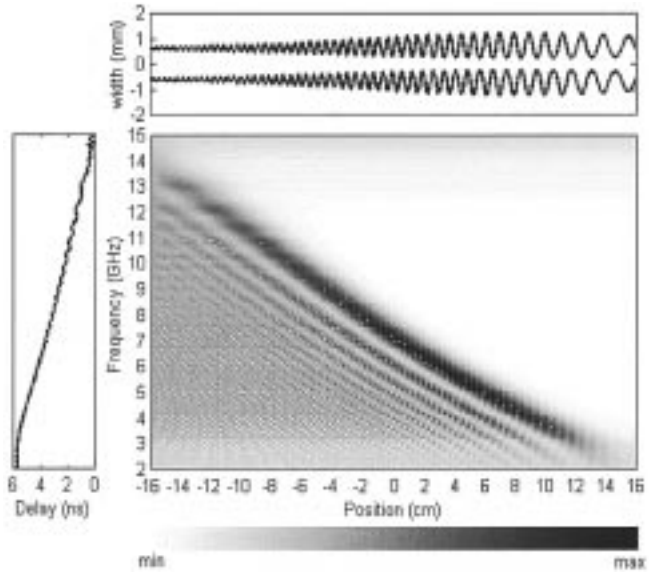

Fig. 2. Average internal power as a function of frequency and position in the CDL using the transmission-line model. Top: CDL strip pattern (not to scale). Left: group-delay.

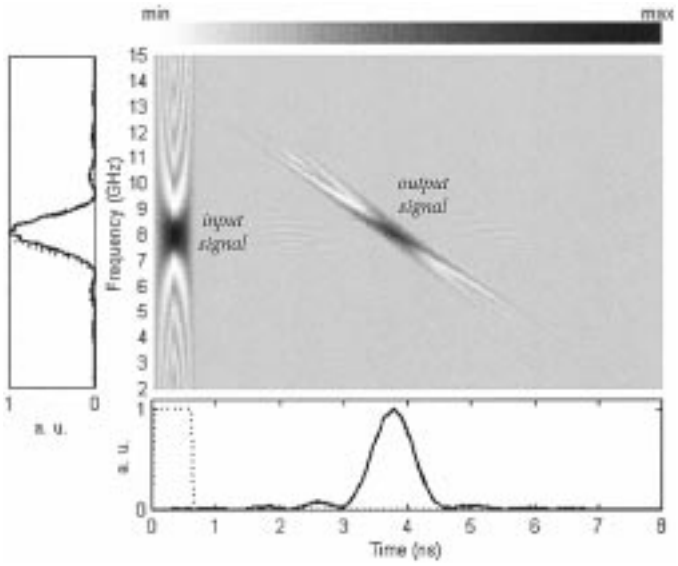

Fig. 3. Bottom: input signal to the CDL (dotted line) and simulation of the output reflected signal (solid line), given in normalized average power (arbitrary units). Top: joint time-frequency representation for the input and output signals (on the right), and normalized input (dotted line) and output (solid line) energy spectral densities (on the left).

This design method, shown here within the constraints of our equipment capabilities, can be applied on higher-dielectric-constant- and thinner substrates to obtain microstrip CDLs some centimeters long with time bandwidth products above several hundreds over very wide frequency ranges. The advantages of these devices are easiness of design, fabrication on a mature technology, and compatibility with monolithic circuits.

Interesting applications as real-time spectral analysis of wideband signals can be envisaged using these devices [7]. The plot at the bottom of Fig. 3 shows an ideal input rectangular pulse 0.6 ns-wide (dotted line), placed within the CDL bandwidth, together with the output pulse reflected from the CDL (solid line), calculated through a numerical simulation using the measured frequency response, both as normalized average power signals (then, only the envelopes of both microwave pulses, traveling on a carrier frequency at 8 GHz, are depicted). The normalized input and output energy spectral densities are the dotted and solid lines, respectively, at the upper left plot. The larger plot of Fig. 3 is a joint time-frequency representation of the energy distributions for both signals providing information of the temporal location of the spectral components. A Wigner-Ville distribution [8] was used in this case. A strong process of linear realignment in time is suffered by the input signal frequencies and, under the assumption of a high delay slope in the signal bandwidth, which is the case for these microstrip CDLs, a single dominant frequency exists at a given instant of time. This way, the output closely reproduces the shape of the energy spectral density, $\sin^2(x)/x^2$, of the input signal on a time axis related to frequency by a linear axis-change given by the CDL delay slope.

IV. Conclusion

We have reported on an easy procedure to design microstrip CDLs with high time-bandwidth products, over frequency ranges of several gigahertzs, consisting in a continuously varying strip width so that the coupling location between the quasi-TEM microstrip mode and the same but counter-propagating mode is linearly distributed in frequency. Measurements have been provided verifying the design method. Fourier processing of wideband signals has been pointed out as a possible application for these devices.

Acknowledgment

The authors would like to thank J. Capmany at the Polytechnic University of Valencia, Spain, for helping them with the prototype measurement.

References

[1] M. Skolnik, *Radar Handbook*, 2nd ed. New York: McGraw-Hill, 1990.
[2] T. Lopetegi, M. A. G. Laso, J. Hernández, M. Bacaicoa, D. Benito, M. J. Garde, M. Sorolla, and M. Guglielmi, "New microstrip wiggly-line filters with spurious passband suppression," *IEEE Trans. Microwave Theory Tech.*, vol. 49, pp. 1593–1598, Sept. 2001.
[3] A. M. Khilla, "Optimum continuous microstrip tapers are amendable to computer aided design," *Microwave J.*, pp. 221–224, May 1983.
[4] M. A. G. Laso, T. Lopetegi, M. J. Erro, D. Benito, M. J. Garde, and M. Sorolla, "Multiple-frequency-tuned photonic bandgap microstrip structures," *IEEE Microwave Guided Wave Lett.*, vol. 10, pp. 220–222, June 2000.
[5] D. M. Pozar, *Microwave Engineering*, 2nd ed. Reading, MA: Addison-Wesley, 1998.
[6] F. Sporleder and H.-G. Unger, *Waveguide Tapers, Transitions and Couplers*. London, U.K.: Peter Peregrinus, 1979.
[7] M. A. G. Laso, T. Lopetegi, M. J. Erro, M. Castillo, D. Benito, M. J. Garde, M. A. Muriel, M. Sorolla, and M. Guglielmi, Real-time spectrum analysis in microstrip technology, in *31st Eur. Microwave Conf.*, London, UK, Sept. 25–27th, 2001. to be presented.
[8] S. Qian and D. Chen, *Joint Time-Frequency Analysis: Methods and Applications*. Englewood Cliffs, NJ: Prentice-Hall, 1996.